Eur. Phys. J. B (2025) 98:169
https://doi.org/10.1140/epjb/s10051-025-01021-1

THE EUROPEAN PHYSICAL JOURNAL B

Research – Solid State and Materials

Diagnosing chaos in a periodically driven Ising model with a ramping field via out-of-time-order correlation saturation

Rohit Kumar Shukla[1,2,3,a], Gaurav Rudra Malik[4,b], S. Aravinda[5,c], and Sunil Kumar Mishra[4,d]

[1] Department of Chemistry, Bar-Ilan University, Ramat-Gan 5290002, Israel
[2] Optics and Quantum Information Group, The Institute of Mathematical Sciences, Chennai 600113, India
[3] Homi Bhabha National Institute, Mumbai 400085, India
[4] Department of Physics, Indian Institute of Technology (Banaras Hindu University), Varanasi 221005, India
[5] Department of Physics, Indian Institute of Technology Tirupati, Tirupati 517619, India

Received 29 March 2025 / Accepted 31 July 2025 / Published online 13 August 2025

Abstract. The dynamic region of out-of-time-ordered correlators (OTOCs) serves as a powerful indicator of chaos in classical and semiclassical systems, capturing the characteristic exponential growth. However, in spin systems, the dynamic region of OTOCs does not reliably quantify chaos as both integrable and chaotic systems display similar behavior. Instead, we utilize the saturation behavior of OTOCs to differentiate between chaotic and integrable regimes. In integrable systems, the saturation region of OTOCs exhibits oscillatory behavior, while in chaotic systems, it shows a stable saturation. To evaluate this distinction, we investigate a time-dependent Ising spin system subjected to a linearly ramping transverse field, analyzing both integrable (without longitudinal field) and non-integrable (with longitudinal field) scenarios. This setup accelerates system ergodicity due to the introduction of an additional time scale within the system, enhancing chaotic dynamics in the non-integrable regime, and provides a compelling model for studying the interplay between integrability and chaos in quantum systems. To further support our findings, we investigate the level spacing distribution of time-dependent unitary operators, which effectively distinguishes chaotic from regular regions in our system and corroborates the results obtained from the saturation behavior of the OTOC. Additionally, we calculate a metric for the normalized Fourier spectrum of the OTOC which is dependent on the number of frequency components present to gain insights into the observed oscillations and its dependence on the ramping field.

1 Introduction

Studying quantum dynamics in many-body systems has been an exciting and challenging frontier in modern physics. Understanding the intricate behavior of quantum correlations, entanglement, and chaos across all dynamical regimes is essential for unlocking the full potential of quantum technologies and shedding light on fundamental aspects of quantum mechanics.

For the class of chaotic dynamics, pioneering research by Larkin and Ovchinnikov delved into the examination of out-of-time-order correlations (OTOCs) as a semiclassical approach to theoretically understand superconductivity [1]. Their study relates the sensitivity of classical trajectories toward the initial conditions to an exponential growth of OTOC. Since then, the concept of OTOC has emerged as a powerful tool to explore the scrambling of information, quantum chaos, butterfly effect [2–8], and phase transition [9–11], providing information about the chaotic nature of the classical and semiclassical systems [2,12]. A notable development in this field is the recent proposal of a quantum information diode that harnesses OTOC [13]. The exponential growth of OTOC represents the chaotic nature of the systems with a classical analog, with its exponent being proportional to the Lyapunov exponent [3]. However, it is not conversely true as despite the exponential growth of OTOC, the system in question may be integrable [14]. Recently, researchers have utilized the norm of the adiabatic gage potential to regulate the adiabatic transitions between eigenstates, revealing its effectiveness as a remarkably sensitive indicator of quantum chaos [15]. The quasiprobability distribution of the OTOC is also used to distinguish between integrable and scrambled systems [16].

[a] e-mail: rohitkrshukla.rs.phy17@itbhu.ac.in (corresponding author)
[b] e-mail: gauravrudramalik.rs.phy22@itbhu.ac.in
[c] e-mail: aravinda@iittp.ac.in
[d] e-mail: sunilkm.app@itbhu.ac.in

The growth of OTOC's has been extensively explored in various spin systems, including Luttinger liquids [17], the XY model [18], the Sachdev–Ye–Kitaev (SYK) model [19], the Heisenberg model, the XXZ model [20,21], integrable transverse field Ising model (TFIM) [22], integrable and non-integrable Floquet system [23]. Numerous experimental approaches for measuring OTOC have been proposed in the literature, spanning a wide range of platforms, such as cold atoms, cavity and circuit quantum electrodynamics (QED), and trapped-ion simulations [8,24–26]. These ideas have paved the way for successful experimental realizations using various systems, such as nuclear spins of molecules [7,10], trapped ions [27,28], and ultra-cold gasses [29]. It is essential to highlight that the observed behavior consistently demonstrates the power law growth of the OTOCs in both integrable and chaotic spin systems [23,30]. This implies that the dynamic region of OTOC does not allow for the differentiation between integrable and chaotic spin systems as it is limited by the finite-dimensional Hilbert space.

The OTOC is frequently discussed in reference to the Floquet spin Hamiltonian driven by time-periodic fields. [23,30,31]. The dynamic and saturation characteristics of OTOCs using the non-local spin block observables for the Floquet Ising model subjected to constant magnetic fields, encompassing both integrable and non-integrable cases, have been studied [23]. Notably, the observed behavior of OTOCs in both integrable and chaotic Floquet systems revealed an approximately quadratic power law growth pattern. If we consider local spin observables, the OTOCs still exhibited a power law growth in their dynamic region in both integrable and chaotic cases [30]. Consequently, we can say that OTOC in constant fields Floquet system calculated using different types of observables like single-spin observables [30], spin block observables [23], and extensive sums of local observables [31], does not provide exponential growth of OTOC irrespective of a chaotic system.

In this work, we explore the behavior of OTOC in a time-dependent Ising spin system under a periodically kicked transverse field, where the field strength increases over time. This setup accelerates the system's randomization, presumably enhancing chaotic dynamics in the non-integrable regime and making the model particularly compelling for our study. We examine both the dynamic and saturation regions of the OTOC, uncovering distinct saturation behaviors that differentiate integrable and chaotic systems.

This paper is structured as follows: we begin by introducing a time-dependent Ising spin system. Next, we define OTOCs and the associated spin observables. We then discuss the level spacing statistics (LSS) within the framework of the system under consideration. Following this, we present our findings. Finally, we conclude by summarizing our main contributions.

2 Theoretical setup and diagnostic tools

2.1 Time-dependent Ising spin system

We consider an Ising chain of length N with open boundary conditions, where the quantum spins are described by Pauli matrices σ_l^x, σ_l^y, and σ_l^z at site l. We apply a time-dependent transverse magnetic field with a magnitude h_z that varies like a straight line with slope Γ and intercept h_{z0}. In the mathematical form, h_z can be represented as $h_z(t) = h_{z0} + \Gamma t$. This field is applied in the form of kicks (represented as integer n) with period τ. A small constant longitudinal magnetic field of amplitude h_{x0} is also applied in order to make the system non-integrable.

The quantum map represents the time evolution operator that evolves the system from $n\tau^+$ to $(n+1)\tau^+$, where τ^+ denotes the time just after τ. The quantum map for a time-dependent Ising spin system is denoted by $\hat{\mathcal{U}}_{xl}(n)$ and is defined as follows (hereafter referred to as the $\hat{\mathcal{U}}_{xl}$ system):

$$\hat{\mathcal{U}}_{xl}(n) = \left[\prod_{l=1}^{N} \exp\left(-i\tau J \hat{\sigma}_l^x \hat{\sigma}_{l+1}^x - i\tau h_x \hat{\sigma}_l^x\right)\right] \left[\prod_{l=1}^{N} \exp(-i\tau h_z(n\tau)\hat{\sigma}_l^z)\right]. \tag{1}$$

Here, J represents the interaction strength between neighboring spins, and h_x/h_z ($h_x = h_{x0}$) is the longitudinal/transverse field. The time evolution of operator $\hat{W}(0)$ after n kicks is defined as $\hat{W}(n) = \hat{U}^\dagger(n)\hat{W}(0)\hat{U}(n)$, where $\hat{U}(n)$ is time evolution operator and defined as $\hat{U}(n) = \hat{\mathcal{U}}_{xl}(1)\hat{\mathcal{U}}_{xl}(2)\hat{\mathcal{U}}_{xl}(3)\ldots\hat{\mathcal{U}}_{xl}(n)$. The amplitude of the transverse field varies with time, rendering the model non-periodic in nature *i.e.,* $\hat{U}(t + n\tau) \neq \hat{U}(t)$.

2.2 Out-of-time-order correlation

Consider two Hermitian observables $\hat{W}(0)$ and $\hat{V}(0)$ at time $t = 0$. After the time evolution of observable $\hat{W}(0)$ *i.e.,* $\hat{W}(t = n\tau)$, it displays noncommutativity with $\hat{V}(0)$ which provides the dynamics of the quantum systems by the spreading of operators under the system's unitary time evolution. This noncommutativity may capture chaotic behavior in the system, which is widely known as OTOC. In mathematical form, OTOC is defined as [1,33]

$$C(n) = -\frac{1}{2}\mathrm{Tr}\left(\hat{\rho}\left[\hat{W}(n), \hat{V}\right]^2\right), \tag{2}$$

where $\hat{\rho}$ is the state of the system, defined as $\hat{\rho} = \frac{e^{-\beta \hat{H}}}{\mathrm{Tr}[e^{-\beta \hat{H}}]}$, with $\beta = \frac{1}{k_B T}$, k_B is the Boltzmann constant and T is the temperature of the system. For our calculation of OTOC, we consider the infinite temperature limit, in which case $\hat{\rho} = \frac{1}{2^N}$. We focus on non-localized observables, defined as follows:

Consider a chain of length N (with N being even) divided into two equal halves. We define an observable $\hat{W}$ over the first half and an observable $\hat{V}$ over the second half. Mathematically, these are given by: $\hat{W} = \frac{2}{N}\sum_{l=1}^{\frac{N}{2}} \hat{\sigma}_l^x$ and $\hat{V} = \frac{2}{N}\sum_{l=\frac{N}{2}+1}^{N} \hat{\sigma}_l^x$. Note that the observables $\hat{W}$ and $\hat{V}$ are *Hermitian but non-unitary*. For such observables, the OTOC, as defined by Eq. (2), can be simplified as follows:

$$C(n) = \frac{1}{2^N}\mathrm{Tr}\left(\hat{W}^2(n)\hat{V}^2\right) - \frac{1}{2^N}\mathrm{Tr}\left(\hat{W}(n)\hat{V}\hat{W}(n)\hat{V}\right). \tag{3}$$

In this expression, the first term is called as the two-point correlation, and the second term is the four-point correlation. Since our observable is non-unitary, the two-point correlation does not reduce to unity. As $n \to \infty$, it asymptotically approaches $\frac{4}{N^2}$, while the four-point correlation tends to zero. Thus, in the long-time limit, $C(\infty) = \frac{4}{N^2}$. The normalized value of the OTOC, $C_N(n)$, relative to its long-time limit is given by $C_N(n) = \frac{C(n)}{C(\infty)}$.

The motivation for considering non-local operators is to increase the Hilbert space dimension of the observables compared to single-site observables. For such observables, information propagation occurs instantly, unlike in localized observables at different positions, allowing for more rapid saturation. Since our focus is on the saturation behavior of the OTOC, we aim to reach the saturation region of the OTOC more quickly.

2.3 Level spacing statistics

The level spacing statistics (LSS) is a concept commonly used in the field of chaos and random matrix theory to study the statistical properties of energy levels of complex systems [34–37]. It provides insights into the level repulsion and clustering behavior of eigenvalues in such systems. The LSS is therefore particularly relevant when studying systems with chaotic and regular dynamics as it characterizes the distribution of spacings between adjacent energy levels, distinguishing a chaotic system from an integrable one [38,39].

In spin systems with constant longitudinal and transverse fields, the Hamiltonian can be used to describe the level statistics of the system. However, when the field is applied in the form of periodic kicks, the Hamiltonian includes a Dirac delta function term, classifying the system as a Floquet system. This delta function term makes it challenging to use the Hamiltonian directly for analyzing the level statistics [40].

In such cases, an alternative approach is employed, which involves the spectral analysis of the unitary operator governing the system's evolution over one period. In Floquet systems, the unitary operator exhibits periodic behavior, *i.e.,* $\hat{\mathcal{U}}_{xl}(t + n\tau) = \hat{\mathcal{U}}_{xl}(t)$. The spectral properties of the system can be fully characterized by the unitary operator for a single period. By taking the logarithm of the eigenvalues of the unitary operator, we obtain the eigenvalues of the system's Hamiltonian, and the level statistics of these eigenvalues represent the statistical behavior of the system [41,42].

If the amplitude of the kicking field varies with time, the evolution becomes aperiodic, meaning $\hat{\mathcal{U}}_{xl}(t+n\tau) \neq \hat{\mathcal{U}}_{xl}(t)$. In this case, the unitary operators for different periods are distinct, and the system's evolution depends on the specific time ordering of the kicks. Consequently, we cannot describe the spectral statistics of the system using the unitary operator for just a single period, as we would in a Floquet system. To accurately describe the spectral statistics for such a system, we must consider the unitary operators for all individual periods. For example, if we want to find the spectral statistics at first, second, and third kicks/period, we would consider the following unitary operators $\hat{U}(1) = \hat{\mathcal{U}}_{xl}(1)$, $\hat{U}(2) = \hat{\mathcal{U}}_{xl}(1)\hat{\mathcal{U}}_{xl}(2)$, and $\hat{U}(3) = \hat{\mathcal{U}}_{xl}(1)\hat{\mathcal{U}}_{xl}(2)\hat{\mathcal{U}}_{xl}(3)$, respectively. We would then calculate the spectral statistics of each of these unitary operators individually to describe the spectral statistics at these three different kicks. If we are interested in the spectral statistics over a larger number of kicks, we would follow a similar process by considering the corresponding unitary operators for each kick.

To accurately calculate the LSS, it is essential to eliminate system symmetries that contribute to degeneracies. In a time-dependent system with a periodic external field and open boundary conditions, reflection symmetry is present. This symmetry can be removed by dividing the eigenvector space into even and odd palindromic subspaces. We generate the Hamiltonian corresponding to either the even or odd palindromic subspace (for details, see Ref. [23]). We then compute the differences between consecutive eigenvalues of the Hamiltonian within any of their subspaces, with these differences forming ensembles denoted as s. After obtaining the ensemble of s, we can draw the distribution of these ensembles. This distribution is known as LSS. If the LSS closely adheres to the Wigner–Dyson (WD) distribution, the system exhibits strong chaotic behavior. The WD distribution is mathematically expressed as [34,43]: $P_W(s) = \frac{\pi s}{2} e^{-\pi s^2/4}$. Conversely, if the LSS exhibits Poisson type, the system is termed nontrivially integrable. The Poisson distribution is given by: $P_P(s) = e^{-s}$.

3 Results

We investigate the OTOC within time-dependent Ising spin systems, considering both integrable and non-

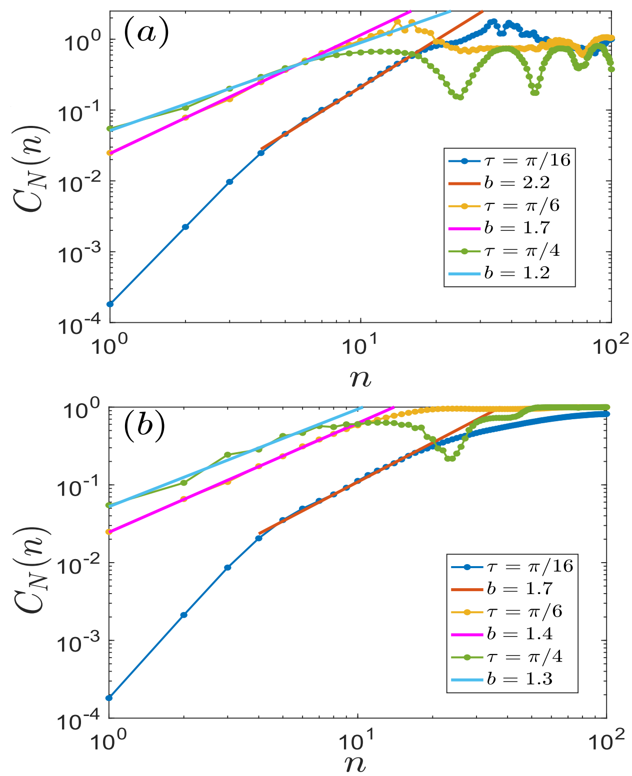

Fig. 1 $C_N(n)$ vs n for (**a**) integrable $\hat{\mathcal{U}}_{0l}$ ($h_{x0} = 0$) (**b**) non-integrable $\hat{\mathcal{U}}_{xl}$ system ($h_{x0} = 1$) for period $\tau = \pi/16$, $\pi/6$, and $\pi/4$. The parameters used for the numerics are $J = 1$, $h_{z0} = 1$, $\Gamma = 0.1$ and $N = 12$. b is the power exponent *i.e.*, $C_N(n) \sim n^b$. The open boundary condition is considered

integrable cases. To calculate the OTOC, we employ non-local observables. OTOC display approximately quadratic power law growth in both integrable (Fig. 1a) and non-integrable systems (Fig. 1b) for a small period *i.e*, $C_N(n) \sim n^b$ where $b \approx 2$, b is known as the power exponent. As the period of the transverse kicks increases, we observe a decrease in the associated exponent of the power law growth. This contrasts with the behavior of the non-integrable system under a constant field, where a longer period leads to an increase in the power law exponent [23]. In the current scenario, there is a time-dependent transverse magnetic field. As the period increases, the transverse kick amplitude becomes rapidly dominant due to its magnitude being defined by $h_z(n\tau) = h_{z0}+n\tau\Gamma$ and saturates in a shorter number of kicks. This in turn leads to a suppression in the growth exponent.

In classical and semiclassical systems, the exponential growth of the OTOC distinguishes chaotic systems from regular ones. However, in spin systems, the emergence of power law growth in both cases has redirected our focus toward a new line of investigation. Instead of focusing on growth, we turned our gaze toward saturation behavior that could potentially serve as a powerful discriminator. As we delve into the saturation behavior of OTOCs, a promising avenue unfolds. Our exploration now centers on how OTOCs saturate – does this behavior differ between integrable and chaotic systems? Can it offer a unique lens through which to distinguish between these two complex regimes? The investigation into the saturation behavior of OTOCs holds immense potential. By meticulously observing how OTOCs saturate, we aim to uncover distinctive patterns that could serve as robust indicators of system behavior. Whether integrable systems showcase different saturation behavior compared to chaotic counterparts is a question that drives our exploration forward.

Let us discuss the saturation behavior of the OTOC in the time-dependent Ising spin systems. We specifically explore three different periods: $\tau = \pi/16$, $\tau = \pi/6$, and $\tau = \pi/4$. We choose $\tau = \pi/16$ for its small size, $\tau = \pi/6$ for its larger size, and $\tau = \pi/4$ as it represents a special point in the Floquet case, showing periodic behavior of OTOC [23,44]. However, in the time-dependent case, it does not exhibit periodic behavior due to the constant (h_x/h_z) being multiplied with the period $\pi/4$, unlike the special case where $h_x = h_z = 1$. In our exploration of the saturation behavior of OTOC, we set the longitudinal field strength from 0 to 1 in increments of 0.1. This approach helps us understand the effect of the longitudinal field in the saturation region of the OTOC. The presence of the longitudinal field makes the system non-integrable. When the

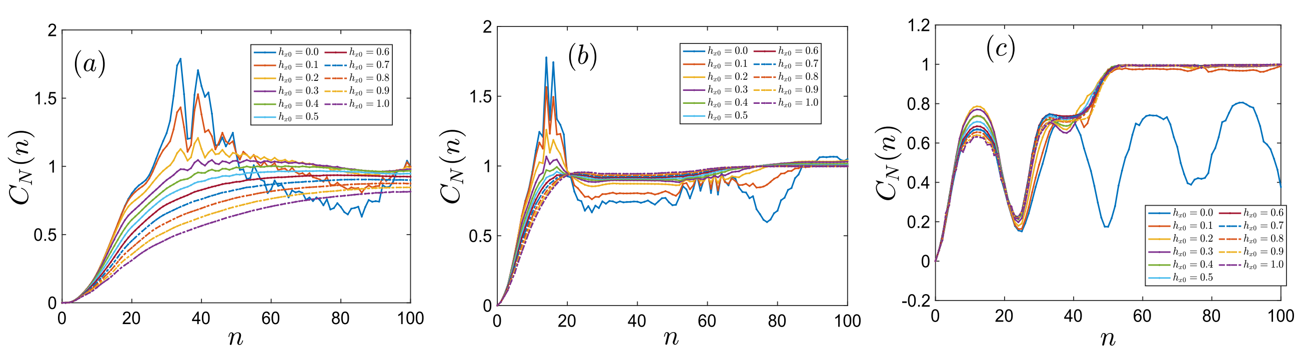

Fig. 2 $C_N(n)$ vs n for different value of h_{x0} lies in between 0 to 1 differing by 0.1 for non-integrable $\hat{\mathcal{U}}_{xl}$ system at period **a** $\tau = \pi/16$, **b** $\tau = \pi/6$, and **c** $\tau = \pi/4$. Other parameters are: $J = 1$, $h_{z0} = 1$, $\Gamma = 0.1$, and $N = 12$. Open boundary conditions are considered

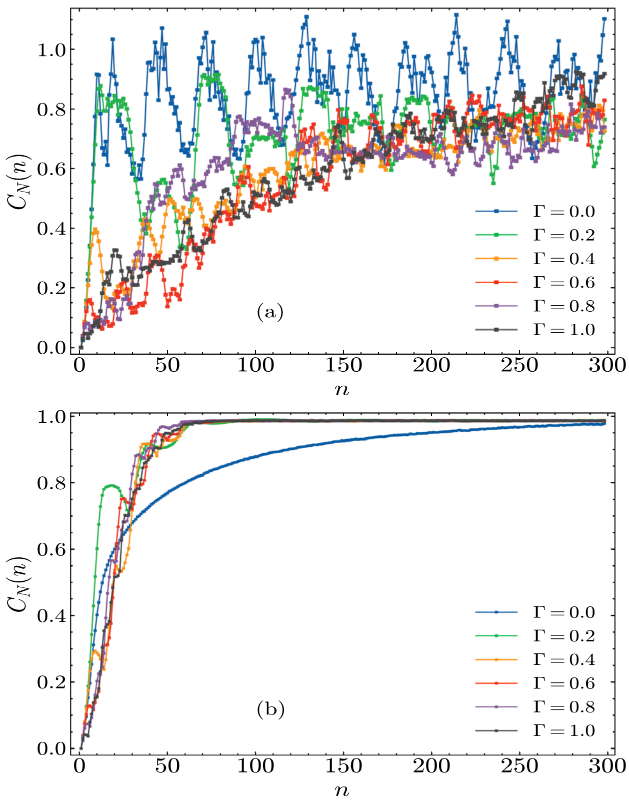

Fig. 3 $C_N(n)$ vs n for **a** integrable $\hat{\mathcal{U}}_{0l}$ and **b** non-integrable $\hat{\mathcal{U}}_{xl}$ system with period $\tau = \pi/6$ at different value of Γ. Other parameters are: $J = 1$, $h_{x0} = 0/1$, $h_{z0} = 1$, and $N = 12$. Open boundary conditions are considered

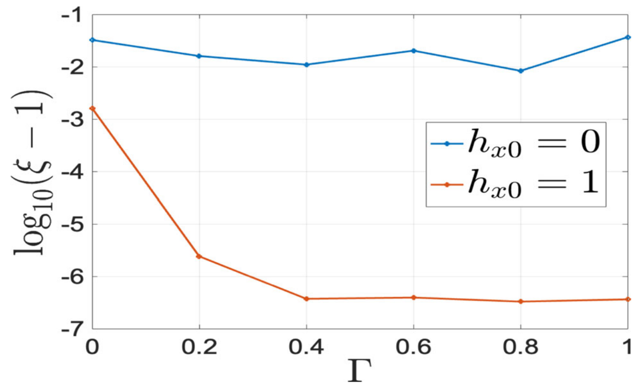

Fig. 4 Fourier space analysis of the OTOC, shown in Fig. **??**a, b, presented as the variation of $\log_{10}(\xi - 1)$ with respect to Γ for a fixed maximum time step $n_{\max} = 300$

longitudinal field is absent, oscillations are present in the OTOC behavior for all periods. However, as we introduce a small longitudinal field term, the oscillation amplitude decreases, and after a certain value of h_{x0}, it saturates at a specific value (Fig. 2a–c). At the period $\tau = \pi/4$, we observe exact saturation in the long-time regime of the OTOC with the introduction of a small longitudinal field term (Fig. 2c). The exact saturation of the OTOC indicates the chaotic behavior of its underlying dynamics. Hence, we may say that a specific value of the longitudinal field term drives the system into chaos.

We also investigate how varying the growth rate of the transverse field, Γ, affects the saturation behavior of the OTOC. Our results show that the OTOC's saturation behavior is independent of Γ. Specifically, in the integrable system, the saturation region of the OTOC exhibits oscillations, while in the non-integrable system, it reaches a stable saturation independent of Γ, as shown in Fig. 4. The OTOC also displays a similar saturation response to changes in the kick period, τ, since τ and the rate Γ act as complementary parameters, with $h_z(t) = h_{z0} + \Gamma n\tau$.

To further understand the effect of the time-dependent field on the OTOC's saturation region, we conduct a quantitative analysis using the inverse participation ratio (IPR), which is discussed in detail below.

Level spacing statistics: To verify the dynamics of our system, we calculate the LSS within the context of time-dependent unitary operators, introducing a novel dimension to spectral analysis. The lack of such an investigation in the existing literature highlights the originality of our approach. In the integrable case, the clustered LSS exhibits a Poisson-type distribution, as illustrated in Fig. 3a, b. However, as we transition to the non-integrable system, a significant transformation occurs–the LSS evolves into a Wigner–Dyson-type distribution, shown in Fig. 3c, d. This shift indicates level repulsion, which is characteristic of quantum chaos. This finding is particularly noteworthy as the relationship between level spacing statistics and the distinction between integrable and chaotic dynamics has been extensively studied primarily in the context of Floquet systems. We observe that even after moving away from the Floquet regime, the results remain consistent, at least for our specific case [41,42].

Fourier Space Analysis:

In our results so far, we have already observed the behavior of the OTOC transform from oscillatory to that of a steady function on transitioning from integrable to the chaotic regime. In order to quantify these observations, we consider the Fourier analysis of the obtained results. To begin with, we may interpret the result obtained in Fig. 2 as a time series, sampled at the rate τ and given as $\{C_k\}_{k=1}^{t_N}$, where t_N denotes the total number of observations. Once we have the individual values of the OTOC at specific periods, we obtain the corresponding discreet Fourier transform, $\{f_j\}_{j=1}^{t_N}$, where $|f_j|$ represents the relative strength of the frequency component $2\pi j/t_N$. To define our metric, taking $\{f_j\}_{j=1}^{t_N}$ as a vector, we rescale the magnitude such that $\sum |f_j|^2 = 1$ by dividing each element with the vector norm. Once normalized, the metric for quantifying the oscillations is given by $\xi = (\sum_j |f_j|^4)^{-1}$, which measures the number of present frequency components. As an example, the OTOC which is a steady function upon saturation has a single 'd.c.' frequency ($f_0 = 1; f_j = 0, j \neq 0$), and thus the value of $\xi = 1$. This is also the minimum possible value of ξ. For an

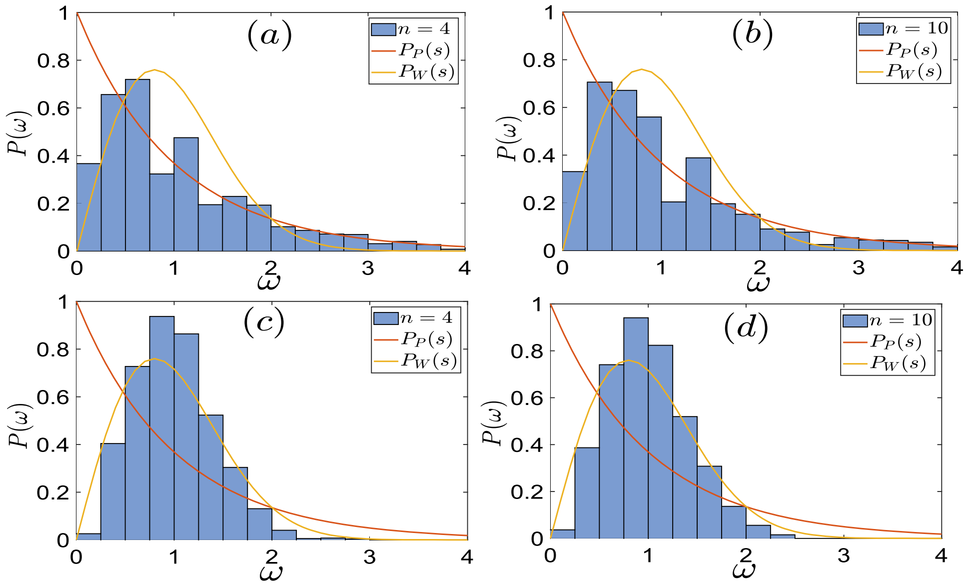

Fig. 5 LSS of the integrable $\hat{\mathcal{U}}_{0l}$ system (a and b), and non-integrable $\hat{\mathcal{U}}_{xl}$ system (c and d) at period $\tau = \pi/4$ in the even Palindromic space at different kicks mentioned in the legend. Other parameters are: $J = 1$, $h_{z0} = 1$, $h_{x0} = 0/1$, $\Gamma = 0.1$, and $N = 12$. Open boundary conditions are considered

oscillating function, there would be a few more frequency components and thereby $\xi > 1$. This follows from normalizing the values, necessarily implying that $\sum |f_j|^4 \leq 1$ (as each $|f_j|^2 \leq 1$) and therefore $\xi \geq 1$. The equality only holds for the signal having only a single frequency component. The manner in which ξ is defined is reminiscent of the inverse participation ration (IPR) measure used in many-body physics to study localization in physical systems. There a high (low) value of IPR indicates the spread of a wavefunction $|\psi\rangle$ over several (few) members of the eigenbasis.

We now apply the metric ξ to the dataset represented in Fig. 2. In all cases corresponding to the chaotic regime (i.e. $h_x > 0.0$), we find that ξ approaches the min. value of 1. Only for $h_x = 0$, does it have a marginally higher value (see Fig. 5 a), dependent on the driving period τ. This quantifies the visual observation regarding the oscillations fading away heading to the chaotic regime. Having this variation, we are now in a position to observe the effect of changing the ramping parameter Γ.

Differentiating the variations observed in Fig. 4a, b, it becomes apparent that even for non-zero values of Γ, the transition away from oscillations toward a steady function remains true going from the integrable to the chaotic regime. However, changing the value of Γ indeed leads to a measurable effect in the chaotic case. From Fig. 5a, it is already apparent that in the saturation region ξ converges to unity as soon as h_x has a value > 0. However, this convergence grows stronger upon increasing the values of Γ along with h_x. To see it, we take the logarithm to base 10 of the quantity $\xi - 1$ (i.e. the deviation of ξ from the minimum value) and find that it decreases from a value of -3 to -6 indicating that the difference between ξ and its minimum value decreases from 10^{-3} to 10^{-6} on increasing Γ from 0 to 1. In contrast, for the integrable case, there are several oscillations present for all values of Γ, validating our metric for the oscillatory behavior of the OTOC. Further, there is no discernible effect of Γ on ξ for the integrable case, where $\xi \approx 1.06$ (within standard errors) for all Γ which is the same value obtained for $\tau = \pi/6, h_x = 0.0$ and $\Gamma = 0.1$ shown in Fig. 5a.

From these observations, we can claim the increasing the rate of growth for the ramping field (by increasing the parameter Γ) takes the system more closer to a constant value of the OTOC, thereby indicating stronger chaotic dynamics. Here we assert that the metric ξ can identify the presence of high-frequency components that normally produce aliasing when exceeding the frequency bound of being half the sampling frequency, as specified by the Shannon–Nyquist theorem. While aliasing does not allow for the reconstruction of the function with the specified frequency components, it is still reflected in the number/magnitude of the Fourier components and thus registered by the metric ξ.

4 Conclusion

We study OTOCs using non-localized observables for a time-dependent Ising spin system. Our focus is on understanding how these OTOCs evolve in the presence and absence of longitudinal fields for the non-integrable/integrable versions of the system, exploring their growth and saturation characteristics.

In both integrable and chaotic cases, we observe a consistent pattern of power law growth in the OTOCs, characterized by a quadratic exponent over shorter periods that diminishes with longer driving periods. Interestingly, the dynamic region reveals no clear distinctions between integrable and chaotic systems, indicating that initial dynamics do not differentiate chaotic behavior. Instead, it is the saturation behavior of the OTOCs that serves as a reliable indicator of system properties: in the integrable system, OTOCs exhibit oscillatory behavior in the saturation regime, while in chaotic systems, they stabilize at a fixed value. This distinction offers a clear criterion for differentiating between the two regimes.

The oscillation in the saturation behavior of OTOC is influenced by the growth rate of the transverse field. However, it is not explicitly determined by the OTOC itself. To address this, we investigate the behavior of IPR in the presence and absence of longitudinal fields. In the absence of the longitudinal field, the IPR takes its maximum value which decreases and saturates as soon as a longitudinal field is applied. Additionally, we observe that as the period of the system increases, the IPR decreases. Our findings further indicate that as the growth rate Γ increases, the value of the IPR is higher compared to the case of $\Gamma = 0$. At $\tau = \pi/4$ with $\Gamma = 0$, there is an exception in both integrable and chaotic systems because at this point IPR value is very high and is governed by the periodic behavior of OTOC.

Validating our results enables us to propose a spectral measure for time-dependent systems. This additional analysis consistently reinforces our earlier observations, providing strong evidence for the distinction between integrable and chaotic systems. In the integrable case, the LSS exhibits Poisson-type behavior, whereas in the chaotic case, it displays Wigner–Dyson-type behavior.

To generalize our results and explore the applicability of our discriminator, we also present findings for the case where both the longitudinal and transverse magnetic fields are time-dependent, represented as cosine and sine waves, respectively. In this scenario, we explore how different observables impact the saturation behavior of the OTOC in the systems with periodic driving fields. Specifically, we consider two types of observables. First, we analyze non-localized observables and localized single-spin observables where the spins are aligned in the x-direction. Corresponding to these scenarios, results are provided in SM-I. Additionally, we consider both non-localized and localized observables oriented in the z-direction. Detailed discussion and the results can be found in SM-II. By doing these analyses, we observe a consistent pattern of saturation behavior. In integrable systems, the OTOCs exhibit oscillatory behavior, while in chaotic systems, they saturate at specific values.

In conclusion, our findings suggest that the saturation behavior of the OTOC can serve as a robust indicator to distinguish between integrable and chaotic systems, irrespective of the specific time-dependent protocol or the choice of observables.

Acknowledgements We would like to acknowledge the support provided by the project "Study of quantum chaos and multipartite entanglement using quantum circuits" sponsored by the Science and Engineering Research Board (SERB), Department of Science and Technology (DST), India under the Core Research Grant CRG/2021/007095

Author contributions

RKS, GRM, SA, and SKM conceived the idea, developed the theory, and conducted the analysis. RKS and GRM performed numerical calculations, interpreted the results, and contributed to the final manuscript.

Funding Information Open access funding provided by Bar-Ilan University.

Data Availability Statement This manuscript has no associated data or the data will not be deposited. [Authors' comment: All the data are already displayed in the figures of the manuscript.]

A Appendix: OTOCs using SBOs and Pauli observables with x-direction alignment in Floquet system with periodic field

Let us discuss the time evolution of the Floquet system, which is defined by the Hamiltonian:

$$\hat{H}(t) = J\hat{H}_{xx} + h_x\hat{H}_x + h_z \sum_{n=-\infty}^{\infty} \delta\left(n - \frac{t}{\tau}\right)\hat{H}_z, \quad (4)$$

In Eq. (4), the longitudinal and transverse fields, h_x and h_z, respectively, are constant.

The wave function under time evolution is defined as follows:

$$\psi(x,t) = \hat{U}(t)\psi(x,0), \quad (5)$$

where $\hat{U}(t)$ is the time evolution operator that evolves the wave function from $t = 0$ to $t = t$. The time-dependent Schrödinger equation is given by

$$i\hbar\frac{\partial\psi}{\partial t} = \hat{H}\psi. \quad (6)$$

Substituting Eq. (5) into Eq. (6), we obtain

$$i\hbar\frac{\partial\hat{U}(t)}{\partial t} = \hat{H}\hat{U}(t). \quad (7)$$

Initially, at $t = 0$, the operator satisfies $\hat{U}(0) = 1$. Since the Hamiltonian $\hat{H}$ is Hermitian, the time evolution operator $\hat{U}(t)$ must be unitary. To prove this, we take the adjoint of Eq. (7):

$$-i\hbar\frac{\partial \hat{U}^{\dagger}(t)}{\partial t} = \hat{U}^{\dagger}(t)\hat{H}. \tag{8}$$

Multiplying Eq. (7) on the left by $\hat{U}^{\dagger}(t)$ and Eq. (8) on the right by $\hat{U}(t)$, and then subtracting the two equations, we get:

$$\frac{\mathrm{d}\left(\hat{U}^{\dagger}(t)\hat{U}(t)\right)}{\mathrm{d}t} = 0. \tag{9}$$

From Eq. (9), it follows that $\hat{U}^{\dagger}(t)\hat{U}(t)$ is a constant. Using the initial condition $\hat{U}(0) = 1$, this constant must be one:

$$\hat{U}^{\dagger}(t)\hat{U}(t) = 1. \tag{10}$$

For periodic time $t = n\tau$, Eq. (5) takes the form for one period:

$$\psi(x,\tau) = \hat{\mathcal{U}}_x(\tau)\psi(x,0). \tag{11}$$

If the unitary operator satisfies the condition $\hat{U}(t+n\tau) = \hat{U}(\tau)$ for $n = 1, 2, \ldots$, the generalized form of the equation for n periods is:

$$\psi(x,n\tau) = [\hat{\mathcal{U}}_x(\tau)]^n\psi(x,0). \tag{12}$$

Thus, the time evolution operator for the periodic system is given by:

$$\hat{U}(n\tau) = [\hat{\mathcal{U}}_x(\tau)]^n. \tag{13}$$

In Floquet systems, fields are applied as kicks in the transverse direction, and the strength of the field is stronger than the interaction field strength J. When the kicking transverse field is applied to the system, the interaction strength has no significant effect. Due to this, the Floquet map is expressed as the product of two exponential terms [45]. For a single period of time, the Floquet map can be expressed as:

$$\hat{\mathcal{U}}(\tau) = \exp\left(-i(\hat{H}_{xx} + \hat{H}_x)\tau\right)\exp(-i\tau h_z\hat{\sigma}_l^z). \tag{14}$$

Let us discuss a more challenging scenario where both the longitudinal and transverse magnetic fields are time-dependent. Unlike the previous case, here, the longitudinal field varies with time. We use both longitudinal and transverse magnetic fields, represented by sine and cosine functions, respectively. Mathematically, they are described as $h_x = h_{x0}\sin(\alpha t)$ and $h_z = h_{z0}\cos(\alpha t)$. The corresponding Hamiltonian for these time-dependent fields is given by

$$\hat{H}(t) = J\hat{H}_{xx} + h_x(t)\hat{H}_x + h_z(t)\sum_{n=-\infty}^{\infty}\delta\left(n - \frac{t}{\tau}\right)\hat{H}_z \tag{15}$$

The quantum map is the time evolution operator that evolves the system between $n\tau^+$ and $(n+1)\tau^+$ where τ^+ indicates the time just after τ. The quantum map for the time-dependent system is given by $\hat{\mathcal{U}}_{xp}(n)$ and defined as (for detailed discussion refer to Refs. [46,47])

$$\hat{\mathcal{U}}_{xp}(n) = \left[\prod_{l=1}^{N}\exp\left(-i\tau\hat{\sigma}_l^x\hat{\sigma}_{l+1}^x - \int_{n\tau}^{(n+1)\tau} h_x(t)\mathrm{d}t\hat{\sigma}_l^x\right)\right]$$
$$\left[\prod_{l=1}^{N}\exp(-i\tau h_z(n\tau)\hat{\sigma}_l^z)\right]. \tag{16}$$

In the Floquet system, fields are constant, and no integration is required, unlike in systems with other time-dependent fields [11,23,30,44]. However, in this case, we introduce a time-dependent longitudinal field. To calculate the unitary operator under such conditions, we must consider small time intervals (bins) between the transverse kicks. To account for the time dependence of the longitudinal field, it is necessary to integrate the longitudinal field over the interval between two kicks. Hereafter, we use the notation $\hat{\mathcal{U}}_{xp}$ and $\hat{\mathcal{U}}_{0p}$ for the non-integrable and integrable cases, respectively. For the calculation of OTOC, we consider the non-localized observables $\hat{W}_B$ and $\hat{V}_B$. At the initial time, $t = 0$, the operators $\hat{W}_B$ and $\hat{V}_B$ commute. However, immediately after n kicks at $t = n\alpha\tau$, the operator $\hat{W}_B(n) = \left(\prod_{k=1}^{n}\hat{U}(k)\right)^{\dagger}\hat{W}_B\left(\prod_{k=1}^{n}\hat{U}(k)\right)$ loses its commutative property. As time progresses, the envelope of the kicked transverse field gradually decreases from its maximum value h_{z0} due to the cosine function. Concurrently, during the same period, the longitudinal field undergoes an increase from 0 to its maximum value h_{x0} due to the sine functions. The frequency of these fields is held constant at $\alpha = \pi/2t_{\max}$, with $t_{\max}$ denoting the duration of the evolution, and in this context, $t_{\max}$ is taken as 16π.

Similar to the main text case, in this case, OTOC displays the power law growth $C_N(n) \sim n^b$ in both integrable and non-integrable systems (Fig. 6a, b). The exponent of this power law is notably high ($b \approx 11$). This observation resonates with prior research, confirming the characteristic behavior of integrable and non-integrable systems [14,23,30].

As we carried out our calculations while varying the system size N, we encountered an intriguing consistency: the growth of the OTOC remained remarkably stable. Within the dynamics regime, these growth patterns consistently remained parallel to each other across different system sizes (Fig. 6c).

In both integrable and non-integrable systems, the dynamic region of the OTOC demonstrates power law growth. However, we find that the dynamic region is unable to effectively discriminate between integrable and chaotic systems. As a result, we shifted our focus to the saturation behavior of the OTOC. In the context of integrable spin systems, the saturation behavior of OTOCs exhibits a unique characteristic oscillation. Specifically, the OTOCs display an asymmetric rise and fall within the saturation regime. Conversely, the non-integrable spin systems paint a different picture. Here, the saturation behavior of OTOCs is marked by exact saturation. Unlike the oscillatory behavior seen in integrable systems, chaotic systems tend to settle into a fixed state at saturation, reflecting the chaotic nature of their dynamics. The intriguing aspect of our investigation lies in the consistency of this behavior across different periods. Whether we examine the systems at one, two, or even three periods $\tau = \pi/16$ (Fig. 7a), $\tau = \pi/6$ (Fig. 7b), and $\tau = \pi/4$ (Fig. 7c), the behavior remains remarkably similar. In our observations, the value of $C_N(n)$ falls within the range of 0 to 2 due to the bounded nature of the asymptotic value of $C_4(n)/C(\infty)$, which remains between -1 and 1 during the post-scrambling phase. Furthermore, the asymptotic value of $C_2(n)/C(\infty)$ converges to 1.

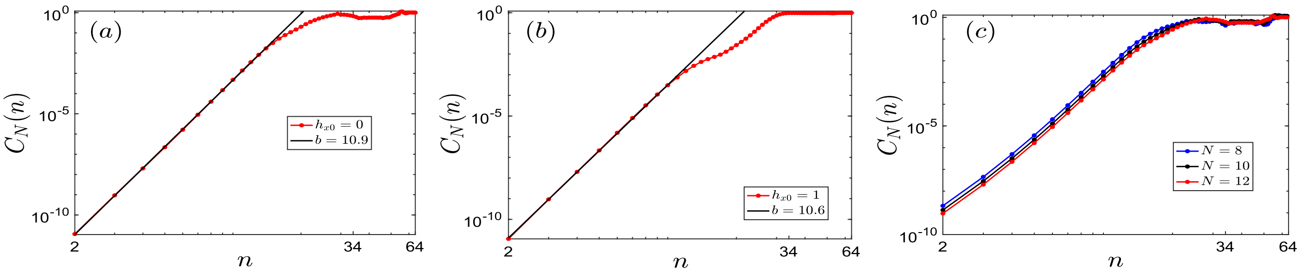

Fig. 6 $C(n)/C(\infty)$ using SBO vs. n (log − log) for **a** integrable $\hat{\mathcal{U}}_{0p}$ and **b** non-integrable $\hat{\mathcal{U}}_{xp}$ system ($h_{x0} = 1$) with system size $N = 12$. **c** $C(n)/C(\infty)$ using SBO vs. n (log − log) for integrable $\hat{\mathcal{U}}_{0p}$ with system size $N = 8, 10$, and 12. Other parameters are: $J = 1$, $h_z = 4$, $t_{\max} = 8\pi$, $\tau = \pi/4$, and $\alpha = \pi/2t_{\max}$. Open boundary conditions are considered

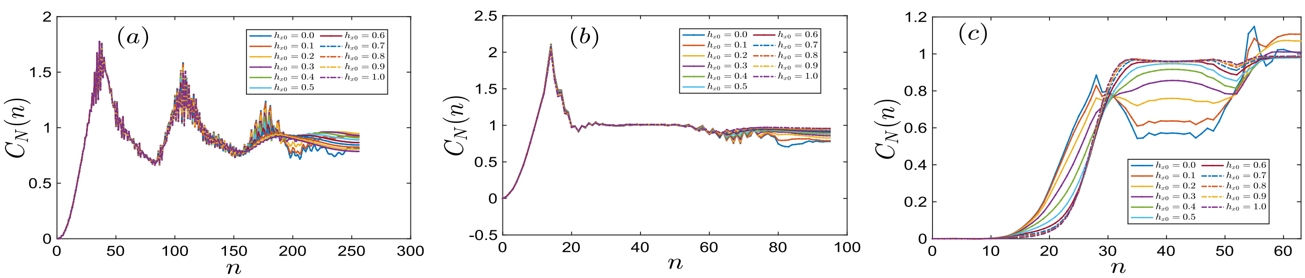

Fig. 7 $C_N(n)$ vs n for different value of h_{x0} lies in between 0 to 1 differing by 0.1 for non-integrable $\hat{\mathcal{U}}_{xp}$ system at period **a** $\tau = \pi/16$, **b** $\tau = \pi/6$, and **c** $\tau = \pi/4$. Other parameters are: $J = 1$, $h_{z0} = 4$, $t_{\max} = 16\pi$, $\alpha = \pi/2t_{\max}$, and system size $N = 12$. Open boundary conditions are considered

We calculate LSS for both integrable and non-integrable time-dependent spin systems by fixing a period of $\tau = \pi/4$. The integrable realm presents us with a consistent observation: Poisson-type behavior in spectral statistics across all numbers of kicks. This consistent pattern reflects an integrable characteristic of the system throughout the time evolution of the system (Fig. 8a–f). However, the non-integrable domain displays a different picture. Initially, the spectral statistics mimic Poisson-type behavior for a certain number of initial kicks. This behavior speaks to the presence of localized modes and partial regularity in the evolution of the system. However, after a distinct number of kicks, a shift occurs to Wigner–Dyson-type behavior, signifying the emergence of chaotic and globally randomized dynamics (Fig. 8g–l). This transition indicates that the system undergoes a transition to chaos after a certain number of kicks. Contrary to the behavior observed in the spin system with a linear field, the system displays a different pattern in the LSS in the spin system with a periodic field. In the linear field case, the system transitions to Wigner–Dyson behavior in the early stages of the evolution, occurring after just a few kicks. This is because the longitudinal field is fixed, while the transverse field starts with an initial small value h_{x0}. This setup initiates a competition between the longitudinal and transverse fields in the initial time regimes. In contrast, with a periodic field, the system shows Wigner–Dyson behavior after some additional kicks. Here, the longitudinal field starts from zero, and the transverse field starts from a high value of $h_x = 4$. Initially, the transverse field dominates over the longitudinal field. However, as time progresses, the transverse field decreases due to its cosine form, while the longitudinal field increases due to its sine form. After some kicks, the effect of the longitudinal field becomes significant.

Subsequently, we extended our study to consider localized Pauli spin observables in the x-direction at positions 1 and $N/2$, *i.e.*, $\hat{W} = \hat{\sigma}_1^x$ and $\hat{V} = \hat{\sigma}_{N/2}^x$. In calculating the OTOC for a localized observable, we focus on the four-point correlation because the two-point correlation can be simplified to the identity operator due to the unitarity of Pauli observables. Consequently, in the limit as n approaches infinity, a four-point correlation tends toward the identity [23]. Therefore, when calculating $C(n)$, it is not necessary to divide by $C(\infty)$. Remarkably, we found consistent saturation behavior of the OTOCs similar to what we observed with the non-localized spin observables. In the integrable case, the OTOCs exhibited oscillating saturation behavior, while in the chaotic case, we again observed exact saturation behavior at different time periods: $\tau = \pi/16$, $\tau = \pi/6$, and $\tau = \pi/4$ (Fig. 9a–c).

B Appendix: OTOCs using non-localized and localized Pauli observables with z-direction alignment in time-dependent Ising spin system

The behavior of OTOC depends on the choice of observables, it is crucial to analyze OTOC with different observables to establish the saturation region as a universal discriminator. To this end, we define non-localized observables aligned in the z-direction as $\hat{W} = \frac{2}{N}\sum_{i=1}^{N/2}\hat{S}_i^z$ and $\hat{V} = \frac{2}{N}\sum_{i=N/2+1}^{N}\hat{S}_i^z$. Our investigations cover both integrable and non-integrable systems under the influence of the operator $\hat{\mathcal{U}}_{xp}$. For the OTOC calculations, we consider

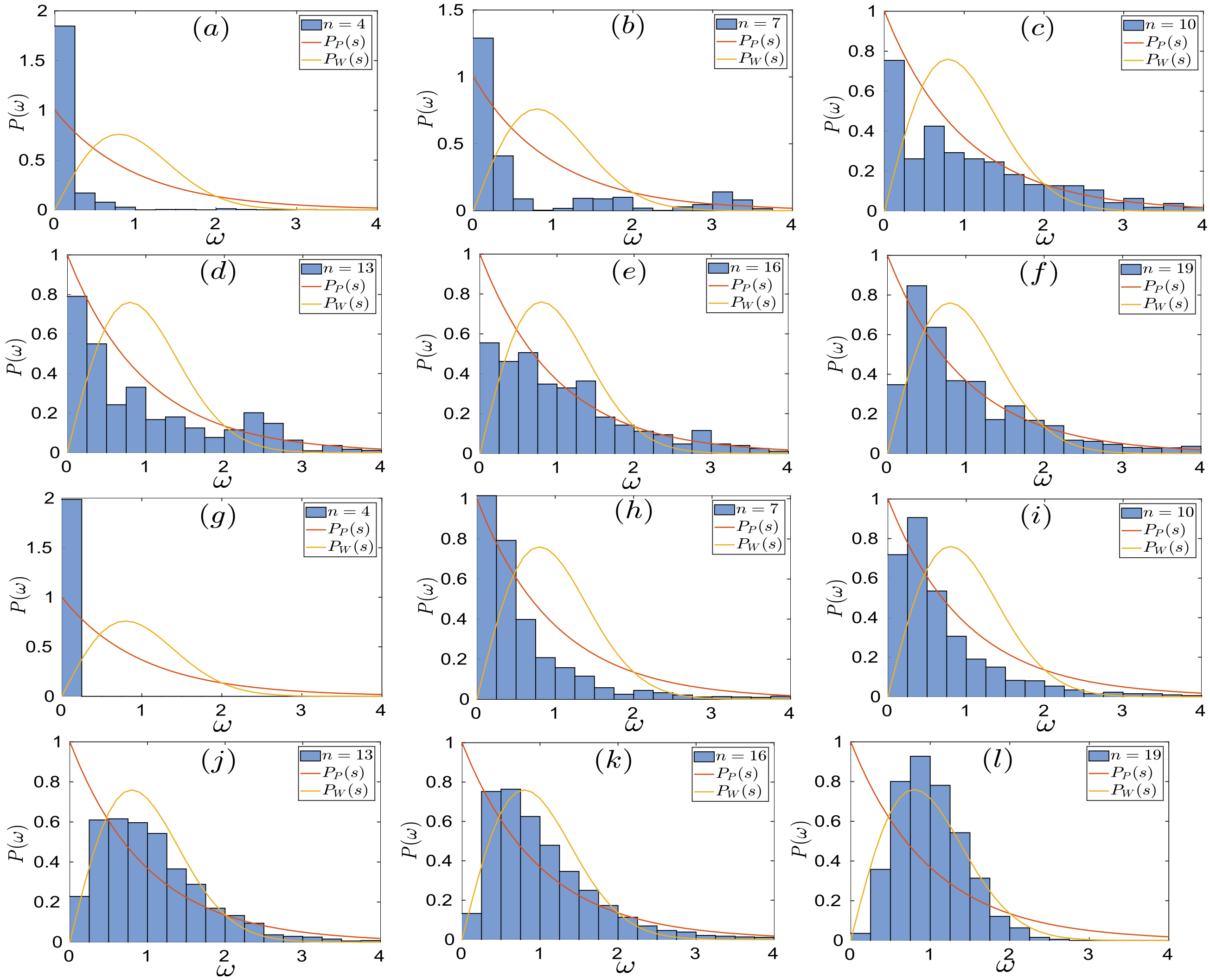

Fig. 8 LSS of the (**a**–**f**) integrable $\hat{\mathcal{U}}_{0p}$ system, and (**g**–**l**) non-integrable $\hat{\mathcal{U}}_{xp}$ system at period $\tau = \pi/4$ in the even Palindromic space at different kicks mentioned in the legend. Other parameters are: $\alpha = \pi/2t_{\max}$, and $t_{\max} = 16\pi$, $J = 1$, $h_{x0} = 0/4, h_{z0} = 4$, $N = 12$. Open boundary conditions are considered

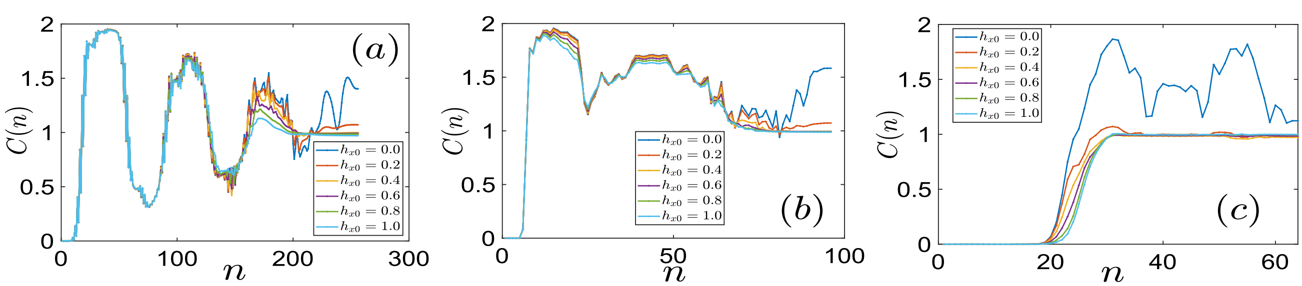

Fig. 9 $C(n)$ ($\hat{W} = \hat{S}_1^x$, and $\hat{V} = \hat{S}_{N/2}^x$) vs n for different value of h_{x0} lies in between 0 to 1 differing by 0.1 for non-integrable $\hat{\mathcal{U}}_{xp}$ system at period **a** $\tau = \pi/16$, **b** $\tau = \pi/6$, and **c** $\tau = \pi/4$. Other parameters are: $J = 1$, $h_{z0} = 4$, $t_{\max} = 16\pi$, $\alpha = \pi/2t_{\max}$, and system size $N = 12$. Open boundary conditions are considered

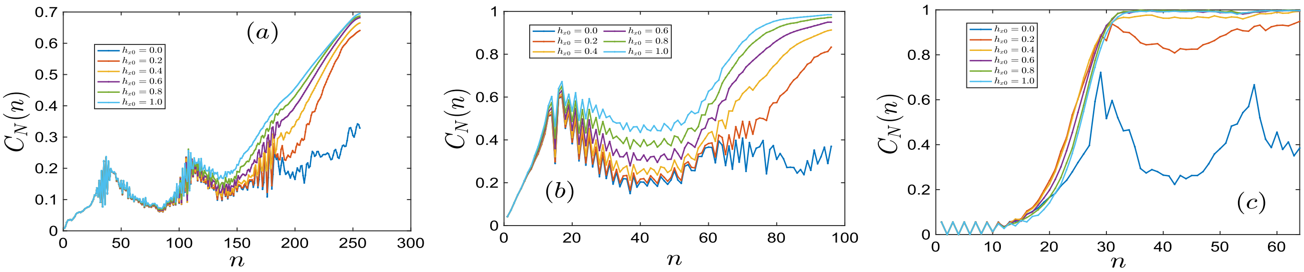

Fig. 10 $C_N(n)$ ($\hat{W} = \sum_{i=1}^{N/2} \hat{S}_i^z$, and $\hat{V} = \sum_{i=N/2+1}^{N} \hat{S}_i^z$) vs n for different value of h_{x0} lies in between 0 to 1 differing by 0.2 for non-integrable $\hat{\mathcal{U}}_{xp}$ system at period **a** $\tau = \pi/16$, **b** $\tau = \pi/6$, and **c** $\tau = \pi/4$. Other parameters are: $J = 1$, $h_{z0} = 4$, $t_{\max} = 16\pi$, $\alpha = \pi/2t_{\max}$, and system size $N = 12$. Open boundary conditions are considered

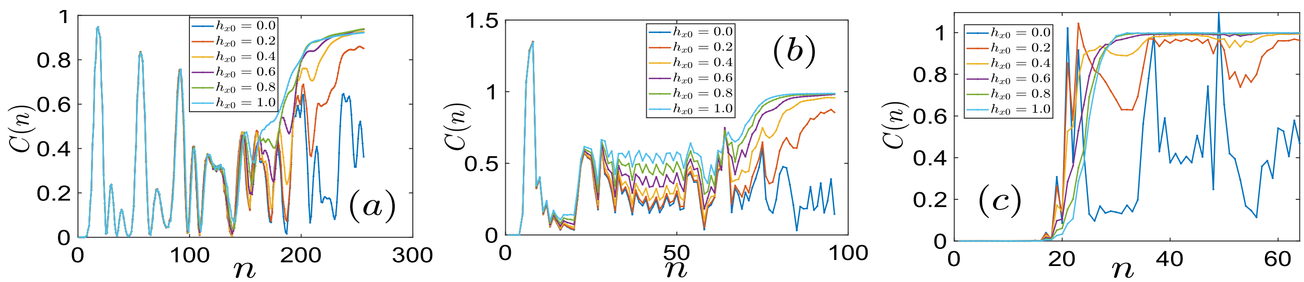

Fig. 11 $C(n)$ ($\hat{W} = \hat{S}_1^z$, and $\hat{V} = \hat{S}_{N/2}^z$) vs n for different value of h_{x0} lies in between 0 to 1 differing by 0.1 for non-integrable $\hat{\mathcal{U}}_{xp}$ system at period **a** $\tau = \pi/16$, **b** $\tau = \pi/6$, and **c** $\tau = \pi/4$. Other parameters are: $J = 1$, $h_{z0} = 4$, $t_{\max} = 16\pi$, $\alpha = \pi/2t_{\max}$, and system size $N = 12$. Open boundary conditions are considered

three periods: $\tau = \pi/16$, $\tau = \pi/6$, and $\tau = \pi/4$. In all cases, we observe the oscillatory behavior of the OTOC in the integrable case, while in the chaotic case, we observe exact saturation behavior (see Fig. 10a–c). When the period is short, the saturation regime of the OTOC shows an increasing trend (see Fig. 10a). However, compared to the integrable case, we observe a non-oscillating behavior in the chaotic case. As the period increases, for large amplitudes of the longitudinal field (around 1), we observe exact saturation (see Fig. 10b, c). This suggests that when the longitudinal field is comparable to the transverse field, the system undergoes in chaotic regime.

Finally, we considered localized Pauli spin observables in the z-direction at positions 1 and $N/2$, *i.e.*, $\hat{W} = \hat{\sigma}_1^z$ and $\hat{V} = \hat{\sigma}_{N/2}^z$. Much like the previous cases, we found consistent saturation behavior of the OTOCs, resembling the behavior seen with the non-localized observables. In the integrable case, the OTOCs displayed oscillating saturation behavior, while in the chaotic case, we again observed exact saturation behavior at different time periods: $\tau = \pi/16$, $\tau = \pi/6$, and $\tau = \pi/4$ (Fig. 11a–c).

References

1. A. Larkin, Y.N. Ovchinnikov, Sov. Phys. JETP **28**, 1200 (1969)
2. R. Prakash, A. Lakshminarayan, Phys. Rev. B **101**, 121108 (2020)
3. E.B. Rozenbaum, S. Ganeshan, V. Galitski, Phys. Rev. Lett. **118**, 086801 (2017)
4. I.L. Aleiner, L. Faoro, L.B. Ioffe, Ann. Phys. **375**, 378 (2016)
5. D.A. Roberts, B. Swingle, Phys. Rev. Lett. **117**, 091602 (2016)
6. Y. Huang, Y.-L. Zhang, X. Chen, Ann. Phys. **529**, 1600318 (2017)
7. K.X. Wei, C. Ramanathan, P. Cappellaro, Phys. Rev. Lett. **120**, 070501 (2018)
8. N.Y. Yao, F. Grusdt, B. Swingle, M.D. Lukin, D.M. Stamper-Kurn, J.E. Moore, and E.A. Demler, arXiv preprint arXiv:1607.01801 (2016)
9. M. Heyl, F. Pollmann, B. Dóra, Phys. Rev. Lett. **121**, 016801 (2018)
10. B. Chen, X. Hou, F. Zhou, P. Qian, H. Shen, N. Xu, Appl. Phys. Lett. **116**, 194002 (2020)
11. R.K. Shukla, G.K. Naik, S.K. Mishra, EPL **132**, 47003 (2021)
12. J. Maldacena, S.H. Shenker, D. Stanford, J. High Energy Phys. **08**, 106 (2016)
13. R.K. Shukla, L. Chotorlishvili, V. Vijayan, H. Verma, A. Ernst, S.S. Parkin, S.K. Mishra, Mater. Quantum Technol. **3**, 035003 (2023)
14. C.-J. Lin, O.I. Motrunich, Phys. Rev. B **97**, 144304 (2018)
15. M. Pandey, P.W. Claeys, D.K. Campbell, A. Polkovnikov, D. Sels, Phys. Rev. X **10**, 041017 (2020)
16. J.R. González Alonso, N. Yunger Halpern, J. Dressel, Phys. Rev. Lett. **122**, 040404 (2019)
17. B. Dóra, R. Moessner, Phys. Rev. Lett. **119**, 026802 (2017)
18. J.-H. Bao, C.-Y. Zhang, Commun. Theoret. Phys. **72**, 085103 (2020)

19. W. Fu, S. Sachdev, Phys. Rev. B **94**, 035135 (2016)
20. J. Riddell, E.S. Sørensen, Phys. Rev. B **99**, 054205 (2019)
21. J. Lee, D. Kim, D.-H. Kim, Phys. Rev. B **99**, 184202 (2019)
22. C.-J. Lin, O.I. Motrunich, Phys. Rev. B **97**, 144304 (2018)
23. R.K. Shukla, A. Lakshminarayan, S.K. Mishra, Phys. Rev. B **105**, 224307 (2022)
24. B. Swingle, G. Bentsen, M. Schleier-Smith, P. Hayden, Phys. Rev. A **94**, 040302 (2016)
25. G. Zhu, M. Hafezi, T. Grover, Phys. Rev. A **94**, 062329 (2016)
26. M. Campisi, J. Goold, Phys. Rev. E **95**, 062127 (2017)
27. K.A. Landsman, C. Figgatt, T. Schuster, N.M. Linke, B. Yoshida, N.Y. Yao, C. Monroe, Nature **567**, 61 (2019)
28. M.K. Joshi, A. Elben, B. Vermersch, T. Brydges, C. Maier, P. Zoller, R. Blatt, C.F. Roos, Phys. Rev. Lett. **124**, 240505 (2020)
29. E.J. Meier, J. Ang'ong'a, F.A. An, B. Gadway, Phys. Rev. A **100**, 013623 (2019)
30. R.K. Shukla, S.K. Mishra, Phys. Rev. A **106**, 022403 (2022)
31. I. Kukuljan, S. Grozdanov, T. Prosen, Phys. Rev. B **96**, 060301 (2017)
32. R.K. Shukla, arXiv preprint arXiv:2505.07550 (2025)
33. K.M. R. Y. Koji Hashimoto, JHEP **138**, (2017)
34. M.L. Mehta, *Random matrices*, 3rd edn. (Academic Press, Cambridge, 2004)
35. L. Santos, J. Phys. A: Math. Gen. **37**, 4723 (2004)
36. E. Bogomolny, B. Georgeot, M.-J. Giannoni, C. Schmit, Phys. Rev. Lett. **69**, 1477 (1992)
37. O. Bohigas, M.-J. Giannoni, C. Schmit, Phys. Rev. Lett. **52**, 1 (1984)
38. Y. Alhassid, R. Levine, Phys. Rev. A **40**, 5277 (1989)
39. T. Prosen, M. Robnik, J. Phys. A: Math. Gen. **26**, 2371 (1993)
40. D. Szász-Schagrin, B. Pozsgay, G. Takács, SciPost Phys. **11**, 037 (2021)
41. A. Lazarides, A. Das, R. Moessner, Phys. Rev. E **90**, 6 (2014)
42. L. D'Alessio and M. Rigol, Phys. Rev. X **4** (2014)
43. L. D'Alessio, Y. Kafri, A. Polkovnikov, M. Rigol, Adv. Phys. **65**, 239 (2016)
44. G.K. Naik, R. Singh, S.K. Mishra, Phys. Rev. A **99**, 032321 (2019)
45. V. Gritsev, A. Polkovnikov, SciPost Phys. **2**, 021 (2017)
46. S.K. Mishra, A. Lakshminarayan, Europhys. Lett. **105**, 10002 (2014)
47. K. Viebahn, Boulder School for Condensed Matter and Materials Physics (2020)